Solving the incompressible surface Navier-Stokes equation by surface finite elements

Sebastian Reuther, and Axel Voigt

Solving the incompressible surface Navier-Stokes equation by surface finite elements

Sebastian Reuther[1] and Axel Voigt[1,2]

[1]*Institute of Scientific Computing, Technische Universität Dresden, Dresden, Germany*
[2]*Dresden Center for Computational Materials Science (DCMS), Dresden, Germany and Center for Systems Biology Dresden (CSBD), Dresden, Germany*

We consider a numerical approach for the incompressible surface Navier-Stokes equation on surfaces with arbitrary genus $g(\mathcal{S})$. The approach is based on a reformulation of the equation in Cartesian coordinates of the embedding $\mathbb{R}^3$, penalization of the normal component, a Chorin projection method, and discretization in space by surface finite elements for each component. The approach thus requires only standard ingredients which most finite element implementations can offer. We compare computational results with discrete exterior calculus simulations on a torus and demonstrate the interplay of the flow field with the topology by showing realizations of the Poincaré-Hopf theorem on *n*-tori. *Published by AIP Publishing.* https://doi.org/10.1063/1.5005142

I. INTRODUCTION

While a huge literature exists for the numerical treatment of the two-dimensional incompressible Navier-Stokes equation in flat space, results for its surface counterpart are rare. The equation has been introduced in Ref. 34 and read for a compact smooth Riemannian surface $\mathcal{S}$ without boundary

$$\partial_t \mathbf{v} + \nabla_{\mathbf{v}} \mathbf{v} = -\text{grad}_{\mathcal{S}}\, p + \frac{1}{\text{Re}} \left(-\mathbf{\Delta}^{\text{dR}} \mathbf{v} + 2\kappa \mathbf{v} \right), \qquad (1)$$

$$\text{div}_{\mathcal{S}}\, \mathbf{v} = 0 \qquad (2)$$

in $\mathcal{S} \times (0, \infty)$ with initial condition $\mathbf{v}(\mathbf{x}, t = 0) = \mathbf{v}_0(\mathbf{x}) \in \mathsf{T}_{\mathbf{x}}\mathcal{S}$, thereby $\mathbf{v}(\mathbf{x}, t) \in \mathsf{T}\mathcal{S}$ denotes the tangential surface velocity, $p(\mathbf{x}, t) \in \mathbb{R}$ denotes the surface pressure, Re denotes the surface Reynolds number, κ denotes the Gaussian curvature, $\mathsf{T}_{\mathbf{x}}\mathcal{S}$ denotes the tangent space on $\mathbf{x} \in \mathcal{S}$, $\mathsf{T}\mathcal{S} = \cup_{\mathbf{x} \in \mathcal{S}} \mathsf{T}_{\mathbf{x}}\mathcal{S}$ denotes the tangent bundle and $\nabla_{\mathbf{v}}$, $\text{grad}_{\mathcal{S}}$, $\text{div}_{\mathcal{S}}$, and $\mathbf{\Delta}^{\text{dR}}$ denote the covariant directional derivative, surface gradient, surface divergence, and surface Laplace-deRham operator, respectively. This intrinsic form of the incompressible surface Navier-Stokes equation is independent of the choice of the coordinate system. Compared with the incompressible Navier-Stokes equation in flat space, not only the operators are replaced by the corresponding surface operators but also an additional contribution from the Gaussian curvature arises. This results from the surface divergence of the surface strain tensor $\mathbf{d} = \frac{1}{2}(\text{grad}_{\mathcal{S}}\, \mathbf{v} + (\text{grad}_{\mathcal{S}}\, \mathbf{v})^T)$, which reads using the Codazzi-Mainardi equation and the incompressibility condition

$$\begin{aligned} 2\, \text{div}_{\mathcal{S}}\, \mathbf{d} &= \text{div}_{\mathcal{S}}(\text{grad}_{\mathcal{S}}\, \mathbf{v}) + \text{div}_{\mathcal{S}}(\text{grad}_{\mathcal{S}}\, \mathbf{v})^T \\ &= -\mathbf{\Delta}^{\text{dR}} \mathbf{v} + \kappa \mathbf{v} + \text{grad}_{\mathcal{S}}(\text{div}_{\mathcal{S}}\, \mathbf{v}) + \kappa \mathbf{v} \\ &= -\mathbf{\Delta}^{\text{dR}} \mathbf{v} + 2\kappa \mathbf{v}. \end{aligned}$$

The unusual sign results from the definition of the surface Laplace-deRham operator.[1] As in flat space, Eqs. (1) and (2) result from conservation of mass and (tangential) linear momentum. Alternatively, the equation can also be derived

from the Rayleigh dissipation potential[10] or as a thin-film limit of the three-dimensional incompressible Navier-Stokes equation.[23]

The incompressible surface Navier-Stokes equation is related to the Boussinesq-Scriven constitutive law for the surface viscosity in two-phase flow problems[7,34,35] and to fluidic biomembranes.[2,3,19,32] Further applications can be found in computer graphics, e.g., Refs. 16, 24, and 37, and geophysics, e.g., Refs. 28 and 33. The equation is also studied as a mathematical problem of its own interest, see, e.g., Refs. 15 and 22. The solution on toroidal surfaces is of special interest for computing plasma motion in fusion plasma physics, see, e.g., Ref. 6.

In contrast to this broad interest, numerical treatments on general surfaces are very rare. In Refs. 27 and 31, a surface vorticity-stream function formulation is introduced. However, this approach cannot deal with harmonic vector fields and is therefore only applicable on surfaces with genus $g(\mathcal{S}) = 0$. The only direct numerical approach for Eqs. (1) and (2), which is also desirable for surfaces with genus $g(\mathcal{S}) \neq 0$, was proposed in Ref. 26 and uses discrete exterior calculus (DEC).

The purpose of this paper is to introduce a surface finite element discretization with only standard ingredients to be applicable on general surfaces. This is achieved by considering an embedding in $\mathbb{R}^3$, extending the variational space from vectors in $\mathsf{T}\mathcal{S}$ to vectors in $\mathbb{R}^3$, and penalizing the normal component. This allows us to split the vector-valued problem into a set of coupled scalar-valued problems for each component for which standard surface finite elements, see the review (Ref. 14), can be used. Similar approaches have already been independently used for other vector-valued problems, see Ref. 18 for a surface vector Laplacian, Ref. 25 for a surface Frank-Oseen problem and Ref. 20 for a surface Stokes problem.

The paper is organized as follows. In Sec. II, we introduce the necessary notation, reformulate the problem in Cartesian

coordinates of the embedding $\mathbb{R}^3$, and introduce the penalization of the normal component. We further modify the equation by rotating the velocity field, which reduces the complexity of the equation. In Sec. III, we describe the numerical approach. For the resulting equations, we propose a Chorin projection approach and a discretization in space by standard piecewise linear Lagrange surface finite elements. We demonstrate the reduction of computational time due to the introduced rotation and validate our approach against a DEC solution on a torus with harmonic vector fields, see Ref. 26. In Sec. IV, results are shown and analyzed on n-tori and conclusions are drawn in Sec. V.

II. MODEL FORMULATION

We follow the same notation as introduced in Ref. 25 and parametrize the surface $\mathcal{S} \subset \mathbb{R}^3$ by the local coordinates θ, φ, i.e.,

$$\mathbf{x} : \mathbb{R}^2 \supset U \to \mathbb{R}^3; \ (\theta, \varphi) \mapsto \mathbf{x}(\theta, \varphi).$$

Thus, the embedded $\mathbb{R}^3$ representation of the surface is given by $\mathcal{S} = \mathbf{x}(U)$. The unit outer normal of $\mathcal{S}$ at point $\mathbf{x}$ is denoted by $\nu(\mathbf{x})$. We denote by $\{\partial_\theta \mathbf{x}, \partial_\varphi \mathbf{x}\}$ the canonical basis to describe the (tangential) velocity $\mathbf{v}(\mathbf{x}) \in \mathsf{T}_\mathbf{x} \mathcal{S}$, i.e., $\mathbf{v} = v^\theta \partial_\theta \mathbf{x} + v^\varphi \partial_\varphi \mathbf{x}$ at a point $\mathbf{x} \in \mathcal{S}$. In a (tubular) neighborhood Ω_δ of $\mathcal{S}$, defined by $\Omega_\delta := \{\widetilde{\mathbf{x}} \in \mathbb{R}^3 : d_\mathcal{S}(\widetilde{\mathbf{x}}) < \frac{1}{2}\delta\}$ with a signed-distance function

$d_\mathcal{S}(\widetilde{\mathbf{x}})$, a coordinate projection $\mathbf{x} \in \mathcal{S}$ of $\widetilde{\mathbf{x}} \in \mathbb{R}^3$ is introduced such that $\widetilde{\mathbf{x}} = \mathbf{x} + d_\mathcal{S}(\widetilde{\mathbf{x}})\nu(\mathbf{x})$. For δ sufficiently small (depending on the local curvature of the surface), this projection is injective, see Ref. 14. For a given $\widetilde{\mathbf{x}} \in \Omega_\delta$, the coordinate projection of $\widetilde{\mathbf{x}}$ will also be called gluing map, denoted by $\pi : \Omega_\delta \to \mathcal{S}, \widetilde{\mathbf{x}} \mapsto \mathbf{x}$. The pressure $p : \mathcal{S} \to \mathbb{R}$ and the velocity $\mathbf{v} : \mathcal{S} \to \mathsf{T}\mathcal{S}$ can be smoothly extended in the neighborhood Ω_δ of $\mathcal{S}$ by utilizing the coordinate projection, i.e., extended fields $\tilde{p} : \Omega_\delta \to \mathbb{R}$ and $\tilde{\mathbf{v}} : \Omega_\delta \to \mathbb{R}^3$ are defined by

$$\tilde{p}(\widetilde{\mathbf{x}}) := p(\mathbf{x}) \quad \text{and} \quad \tilde{\mathbf{v}}(\widetilde{\mathbf{x}}) := \mathbf{v}(\mathbf{x}), \tag{3}$$

respectively, for $\widetilde{\mathbf{x}} \in \Omega_\delta$ and $\mathbf{x}$ the corresponding coordinate projection. To embed the $\mathbb{R}^3$ vector space structure to the tangential bundle of the surface, we use the pointwise defined normal projection

$$\pi_\mathcal{S}(\mathbf{x}) : \mathsf{T}_\mathbf{x}\mathbb{R}^3 \cong \mathbb{R}^3 \to \mathsf{T}_\mathbf{x}\mathcal{S};$$
$$\widehat{\mathbf{v}}(\mathbf{x}) \mapsto \widehat{\mathbf{v}}(\mathbf{x}) - \nu(\mathbf{x})(\nu(\mathbf{x}) \cdot \widehat{\mathbf{v}}(\mathbf{x})) = \mathbf{v}(\mathbf{x}),$$

for all $\mathbf{x} \in \mathcal{S}$, which maps the $\mathbb{R}^3$ velocity $\widehat{\mathbf{v}} = v_x \mathbf{e}^x + v_y \mathbf{e}^y + v_z \mathbf{e}^z \in \mathbb{R}^3$, not necessarily tangential to the surface, to the tangential velocity $\mathbf{v} \in \mathsf{T}_\mathbf{x}\mathcal{S}$. We drop the argument $\mathbf{x}$ when applied to velocity fields living on $\mathcal{S}$. With these notations, we have the following correspondence of the different representations of first order differential operators on surfaces:

$\dfrac{\mathsf{T}\mathcal{S}}{\mathbb{R}^3}$	$\dfrac{\text{grad}_\mathcal{S} p}{\pi_\mathcal{S} \nabla p}$	$\dfrac{\text{rot}_\mathcal{S} p}{\nu \times \nabla p}$	$\dfrac{\text{div}_\mathcal{S} \mathbf{v}}{\nabla \cdot \widehat{\mathbf{v}} - \nu \cdot (\nabla \widehat{\mathbf{v}} \cdot \nu) - \mathcal{H}(\widehat{\mathbf{v}} \cdot \nu)}$	$\dfrac{\text{rot}_\mathcal{S} \mathbf{v}}{(\nabla \times \widehat{\mathbf{v}}) \cdot \nu}$

thereby $\mathcal{H}$ denotes the mean curvature. We further define $\text{div}_\mathcal{S} \widehat{\mathbf{v}} = \nabla \cdot \widehat{\mathbf{v}} - \nu \cdot (\nabla \widehat{\mathbf{v}} \cdot \nu)$ and $\text{rot}_\mathcal{S} \widehat{\mathbf{v}} = (\nabla \times \widehat{\mathbf{v}}) \cdot \nu = -\text{div}_\mathcal{S}(\nu \times \widehat{\mathbf{v}})$, see Ref. 27, and thus obtain

$$\nabla_\mathbf{v} \mathbf{v} = \frac{1}{2} \text{grad}_\mathcal{S}(\mathbf{v} \cdot \mathbf{v}) + \text{rot}_\mathcal{S} \mathbf{v} \nu \times \mathbf{v}$$
$$= \frac{1}{2} \text{grad}_\mathcal{S}(\widehat{\mathbf{v}} \cdot \widehat{\mathbf{v}}) + \text{rot}_\mathcal{S} \widehat{\mathbf{v}} \nu \times \widehat{\mathbf{v}}.$$

Using the definition of Ref. 1, the surface Laplace-deRham operator reads $\Delta^{\text{dR}}\mathbf{v} = -\left(\Delta^{\text{RR}} + \Delta^{\text{GD}}\right)\mathbf{v}$ with $\Delta^{\text{RR}}\mathbf{v} = \text{rot}_\mathcal{S} \text{rot}_\mathcal{S} \mathbf{v}$ and $\Delta^{\text{GD}}\mathbf{v} = \text{grad}_\mathcal{S} \text{div}_\mathcal{S} \mathbf{v}$. In analogy, we define $\widehat{\Delta}^{\text{dR}}\widehat{\mathbf{v}} = -(\text{rot}_\mathcal{S} \text{rot}_\mathcal{S} \widehat{\mathbf{v}} + \text{grad}_\mathcal{S} \text{div}_\mathcal{S} \widehat{\mathbf{v}})$. In Ref. 25, it has been shown that $\Delta^{\text{dR}}\mathbf{v} \approx \widehat{\Delta}^{\text{dR}}\widehat{\mathbf{v}}$ if the normal component $(\widehat{\mathbf{v}} \cdot \nu)$ is penalized by an additional term $\alpha(\nu \cdot \widehat{\mathbf{v}})\nu$. First order convergence in the penalty parameter α was numerically shown for this approximation. Due to the incompressibility, we thus obtain $\Delta^{\text{dR}}\mathbf{v} = -\text{rot}_\mathcal{S} \text{rot}_\mathcal{S} \mathbf{v} \approx -\text{rot}_\mathcal{S} \text{rot}_\mathcal{S} \widehat{\mathbf{v}}$, and the approximation of the surface incompressible Navier-Stokes equation in Cartesian coordinates reads

$$\partial_t \widehat{\mathbf{v}} + \text{rot}_\mathcal{S} \widehat{\mathbf{v}} \nu \times \widehat{\mathbf{v}} = -\text{grad}_\mathcal{S} \bar{p} + \frac{1}{\text{Re}} \left(-\text{rot}_\mathcal{S} \text{rot}_\mathcal{S} \widehat{\mathbf{v}} + 2\kappa\widehat{\mathbf{v}}\right)$$
$$- \alpha(\widehat{\mathbf{v}} \cdot \nu)\nu, \tag{4}$$
$$\text{div}_\mathcal{S} \widehat{\mathbf{v}} = 0 \tag{5}$$

with $\bar{p} = p + \frac{1}{2}\widehat{\mathbf{v}} \cdot \widehat{\mathbf{v}}$. This formulation ensures the velocity to be tangential only weakly through the added penalty term and is equivalent to Eqs. (1) and (2) only if $\widehat{\mathbf{v}} \cdot \nu = 0$.

The advantage of Eqs. (4) and (5) is that they can be solved for each component v_x, v_y, v_z, and $\bar{p}$ using standard approaches for scalar-valued problems on surfaces, such as the surface finite element method,[11,12,14] level-set approaches,[5,13,17,36] diffuse interface approximations,[29] or trace finite element methods.[30] However, the $\text{rot}_\mathcal{S} \text{rot}_\mathcal{S} \widehat{\mathbf{v}}$ term leads to a heavy workload in terms of implementation and assembly time, as 36 second order operators, 72 first order operators, and 36 zero order operators have to be considered. This effort can drastically be reduced by rotating the velocity field in the tangent plane. Instead of $\widehat{\mathbf{v}}$ we consider $\widehat{\mathbf{w}} = \nu \times \widehat{\mathbf{v}}$ as unknown. Applying $\nu\times$ to Eq. (4), we thus obtain

$$\partial_t \widehat{\mathbf{w}} - \text{div}_\mathcal{S} \widehat{\mathbf{w}} \nu \times \widehat{\mathbf{w}} = -\text{rot}_\mathcal{S} \tilde{p} + \frac{1}{\text{Re}} \left(\text{grad}_\mathcal{S} \text{div}_\mathcal{S} \widehat{\mathbf{w}} + 2\kappa\widehat{\mathbf{w}}\right)$$
$$- \alpha(\widehat{\mathbf{w}} \cdot \nu)\nu, \tag{6}$$
$$\text{rot}_\mathcal{S} \widehat{\mathbf{w}} = 0 \tag{7}$$

where we have used the identities $\text{rot}_\mathcal{S} \widehat{\mathbf{v}} = -\text{div}_\mathcal{S} \widehat{\mathbf{w}}$, $\text{div}_\mathcal{S} \widehat{\mathbf{v}} = \text{rot}_\mathcal{S} \widehat{\mathbf{w}}$, $\widehat{\mathbf{v}} = -\nu \times \widehat{\mathbf{w}}$, and $\nu \times (\nu \times \widehat{\mathbf{v}}) = -\widehat{\mathbf{v}}$. The $\text{grad}_\mathcal{S} \text{div}_\mathcal{S} \widehat{\mathbf{w}}$ term now contains only 9 second order terms and the remaining terms are of similar complexity as in Eqs. (4) and (5). An alternative form proposed in Ref. 20 for a surface Stokes problem is based on the identity for the surface strain tensor $\mathbf{d} = \frac{1}{2}\pi_\mathcal{S}(\nabla\widehat{\mathbf{v}} + (\nabla\widehat{\mathbf{v}})^T)\pi_\mathcal{S}$. This formulation is analytically more trackable. However, it is expected to be computationally more involved as the resulting system contains 18 second order

terms. Another disadvantage might be the hidden dependency of the velocity on geometric properties. Detailed parameter studies to demonstrate the influence of the Gaussian curvature as considered in Refs. [26] and [31] will be less straight forward.

III. DISCRETIZATION

A. Time discretization

Let $0 < t_0 < t_1 < \ldots$ be a sequence of discrete times with time step width $\tau_n := t_{n+1} - t_n$ in the n-th iteration. The fields $\widehat{\mathbf{v}}^n(\mathbf{x}) = \widehat{\mathbf{v}}(\mathbf{x}, t_n)$, $\widehat{\mathbf{w}}^n(\mathbf{x}) = \widehat{\mathbf{w}}(\mathbf{x}, t_n)$, and $\bar{p}^n(\mathbf{x}) = \bar{p}(\mathbf{x}, t_n)$ correspond to the time-discrete functions at t_n. Applying a Chorin projection method[8] to Eqs. (4) and (5) with a semi-implicit Euler time scheme results in time discrete systems of equations as follows:

Problem 1. *Let* $\widehat{\mathbf{v}}^0 \in C(\mathcal{S}; \mathbb{R}^3)$ *be a given initial velocity field with* $\widehat{\mathbf{v}}^0 = \mathbf{v}^0$. *For* $n = 0, 1, 2, \ldots$ *find*

1. $\widehat{\mathbf{v}}^*$ *such that*

$$\frac{1}{\tau_n}(\widehat{\mathbf{v}}^* - \widehat{\mathbf{v}}^n) = -\operatorname{rot}_{\mathcal{S}} \widehat{\mathbf{v}}^* \boldsymbol{\nu} \times \widehat{\mathbf{v}}^n + \frac{1}{\mathrm{Re}} \left(-\operatorname{rot}_{\mathcal{S}} \operatorname{rot}_{\mathcal{S}} \widehat{\mathbf{v}}^* + 2\kappa \widehat{\mathbf{v}}^* \right)$$
$$- \alpha(\widehat{\mathbf{v}}^* \cdot \boldsymbol{\nu})\boldsymbol{\nu},$$

2. $\bar{p}^{n+1}$ *such that*

$$\tau_n \Delta_{\mathcal{S}} \bar{p}^{n+1} = \operatorname{div}_{\mathcal{S}} \widehat{\mathbf{v}}^*,$$

3. $\widehat{\mathbf{v}}^{n+1}$ *such that*

$$\widehat{\mathbf{v}}^{n+1} = \widehat{\mathbf{v}}^* - \tau_n \operatorname{grad}_{\mathcal{S}} \bar{p}^{n+1},$$

with $\Delta_{\mathcal{S}}$ *being the Laplace-Beltrami operator.*

The corresponding scheme for Eqs. (6) and (7) follows by defining $\widehat{\mathbf{w}}^* = \boldsymbol{\nu} \times \widehat{\mathbf{v}}^*$ and applying $\boldsymbol{\nu} \times$ to the equation in the first step. We thus obtain the following:

Problem 2. *Let* $\widehat{\mathbf{v}}^0 \in C(\mathcal{S}; \mathbb{R}^3)$ *be a given initial velocity field with* $\widehat{\mathbf{v}}^0 = \mathbf{v}^0$. *Compute* $\widehat{\mathbf{w}}^0 = \boldsymbol{\nu} \times \widehat{\mathbf{v}}^0$. *For* $n = 0, 1, 2, \ldots$ *find*

1. $\widehat{\mathbf{w}}^*$ *such that*

$$\frac{1}{\tau_n}(\widehat{\mathbf{w}}^* - \widehat{\mathbf{w}}^n) = \operatorname{div}_{\mathcal{S}} \widehat{\mathbf{w}}^* \boldsymbol{\nu} \times \widehat{\mathbf{w}}^n + \frac{1}{\mathrm{Re}} \left(\operatorname{grad}_{\mathcal{S}} \operatorname{div}_{\mathcal{S}} \widehat{\mathbf{w}}^* + 2\kappa \widehat{\mathbf{w}}^* \right)$$
$$- \alpha(\widehat{\mathbf{w}}^* \cdot \boldsymbol{\nu})\boldsymbol{\nu},$$

2. $\bar{p}^{n+1}$ *such that*

$$\tau_n \Delta_{\mathcal{S}} \bar{p}^{n+1} = \operatorname{rot}_{\mathcal{S}} \widehat{\mathbf{w}}^*,$$

3. $\widehat{\mathbf{w}}^{n+1}$ *such that*

$$\widehat{\mathbf{w}}^{n+1} = \widehat{\mathbf{w}}^* - \tau_n \operatorname{rot}_{\mathcal{S}} \bar{p}^{n+1},$$

4. $\widehat{\mathbf{v}}^{n+1} = -\boldsymbol{\nu} \times \widehat{\mathbf{w}}^{n+1}$.

For simplicity, we consider only a Taylor-0 linearization of the nonlinear term in both problems.

B. Space discretization

For the discretization in space, we apply the surface finite element method for scalar-valued problems[14] for each component. Therefore, the surface $\mathcal{S}$ is discretized by a conforming triangulation $\mathcal{S}_h$, given as the union of simplices, i.e., $\mathcal{S}_h := \bigcup_{T \in \mathcal{T}} T$. We use globally continuous, piecewise linear Lagrange surface finite elements

$$\mathbb{V}_h(\mathcal{S}_h) = \left\{ v_h \in C^0(\mathcal{S}_h) : v_h|_T \in \mathbb{P}^1, \forall T \in \mathcal{T} \right\}$$

as trial and test space for all components $\widehat{v}_i$ of $\widehat{\mathbf{v}}$ as well as $\widehat{w}_i$ of $\widehat{\mathbf{w}}$ and $\bar{p}$ with $\mathcal{T}$ the set of triangular faces.

The resulting fully discrete problem for Problem 1 reads as follows: For $n = 0, 1, 2, \ldots$ find $\widehat{v}_i^*, \bar{p}^{n+1} \in \mathbb{V}_h(\mathcal{S}_h)$ such that $\forall \widehat{u}_i, \widehat{q} \in \mathbb{V}_h(\mathcal{S}_h)$,

$$\frac{1}{\tau_n} \int_{\mathcal{S}_h} \widehat{v}_i^* \widehat{u}_i \, d\mathcal{S} + \int_{\mathcal{S}_h} \operatorname{rot}_{\mathcal{S}} \widehat{\mathbf{v}}^* \left(\boldsymbol{\nu} \times \widehat{\mathbf{v}}^n \right)_i \widehat{u}_i \, d\mathcal{S}$$
$$+ \alpha \int_{\mathcal{S}_h} \boldsymbol{\nu} \cdot \widehat{\mathbf{v}}^* \nu_i \widehat{u}_i \, d\mathcal{S} - \frac{1}{\mathrm{Re}} \int_{\mathcal{S}_h} \operatorname{rot}_{\mathcal{S}} \widehat{\mathbf{v}}^* \operatorname{rot}_{\mathcal{S}} \left(\widehat{u}_i \mathbf{e}^i \right) \, d\mathcal{S}$$
$$- 2 \int_{\mathcal{S}_h} \kappa \widehat{v}_i^* \widehat{u}_i \, d\mathcal{S} = \frac{1}{\tau_n} \int_{\mathcal{S}_h} \widehat{v}_i^n \widehat{u}_i \, d\mathcal{S}, \qquad (8)$$

$$\tau_n \int_{\mathcal{S}_h} \operatorname{grad}_{\mathcal{S}} \bar{p}^{n+1} \cdot \operatorname{grad}_{\mathcal{S}} \widehat{q} \, d\mathcal{S} + \int_{\mathcal{S}_h} \widehat{\mathbf{v}}^* \cdot \operatorname{grad}_{\mathcal{S}} \widehat{q} \, d\mathcal{S} = 0, \quad (9)$$

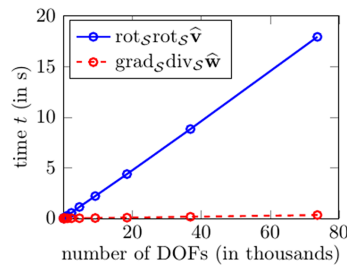| number of DOFs	time $t_{\widehat{\mathbf{v}}}$ (in ms)	time $t_{\widehat{\mathbf{w}}}$ (in ms)	time ratio $t_{\widehat{\mathbf{v}}}/t_{\widehat{\mathbf{w}}}$
4614	1123.39	15.56	72.2
9222	2199.54	31.62	69.6
18438	4368.73	69.05	63.3
36870	8817.76	156.68	56.3
73734	17920.00	326.54	54.9

FIG. 1. Assembly times $t_{\widehat{\mathbf{v}}}$ and $t_{\widehat{\mathbf{w}}}$ for the 2 s order operators $\operatorname{rot}_{\mathcal{S}} \operatorname{rot}_{\mathcal{S}} \widehat{\mathbf{v}}$ and $\operatorname{grad}_{\mathcal{S}} \operatorname{div}_{\mathcal{S}} \widehat{\mathbf{w}}$ as a function of the number of DOFs.
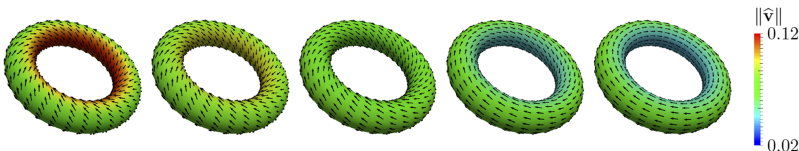
FIG. 2. Numerical solution of $\widehat{\mathbf{v}} = -\boldsymbol{\nu} \times \widehat{\mathbf{w}}$ at $t = 0, 2, 10, 30$, and 60 (left to right). The color indicates the absolute value of the velocity $\widehat{\mathbf{v}}$. The arrows are rescaled for better visualization.
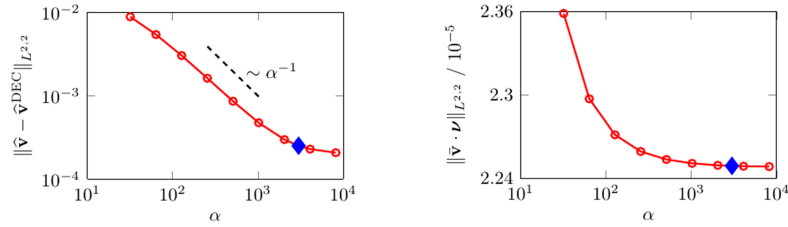
FIG. 3. $L^{2,2}$ norm of the error between the present velocity field $\widehat{\mathbf{v}}$ and the velocity field $\widehat{\mathbf{v}}^{DEC}$ computed with DEC against the penalty parameter α (left) and $L^{2,2}$ norm of the normal component of the rescaled velocity field $\bar{\mathbf{v}} = \widehat{\mathbf{v}}/\|\widehat{\mathbf{v}}\|_{L^2}$ against the penalty parameter α (right). The first superscript index denotes the L^p norm regarding time t and the second superscript index denotes the spatial L^p norm. The blue diamond indicates the penalty parameter α used for visualization in Fig. 2 and in the following examples.

for $i = x, y, z$, from which $\widehat{\mathbf{v}}^{n+1}$ can be computed according to step 3 in Problem 1.

The resulting fully discrete problem for Problem 2 reads as follows: For $n = 0, 1, 2, \ldots$ find $\widehat{w}_i^*, \bar{p}^{n+1} \in \mathbb{V}_h(\mathcal{S}_h)$ such that $\forall \widehat{u}_i, \widehat{q} \in \mathbb{V}_h(\mathcal{S}_h)$,

$$\frac{1}{\tau_n} \int_{\mathcal{S}_h} \widehat{w}_i^* \widehat{u}_i \, d\mathcal{S} - \int_{\mathcal{S}_h} \text{div}_{\mathcal{S}} \widehat{\mathbf{w}}^* (\boldsymbol{\nu} \times \widehat{\mathbf{w}}^n)_i \widehat{u}_i \, d\mathcal{S}$$

$$+ \alpha \int_{\mathcal{S}_h} \boldsymbol{\nu} \cdot \widehat{\mathbf{w}}^* \nu_i \widehat{u}_i \, d\mathcal{S} + \frac{1}{\text{Re}} \int_{\mathcal{S}_h} \text{div}_{\mathcal{S}} \widehat{\mathbf{w}}^* (\text{grad}_{\mathcal{S}} \widehat{u}_i)_i \, d\mathcal{S}$$

$$- 2 \int_{\mathcal{S}_h} \kappa \widehat{w}_i^* \widehat{u}_i \, d\mathcal{S} = \frac{1}{\tau_n} \int_{\mathcal{S}_h} \widehat{w}_i^n \widehat{u}_i \, d\mathcal{S}, \tag{10}$$

$$\tau_n \int_{\mathcal{S}_h} \text{grad}_{\mathcal{S}} \bar{p}^{n+1} \cdot \text{grad}_{\mathcal{S}} \widehat{q} \, d\mathcal{S}$$

$$+ \int_{\mathcal{S}_h} \boldsymbol{\nu} \times \widehat{\mathbf{w}}^* \cdot \text{grad}_{\mathcal{S}} \widehat{q} \, d\mathcal{S} = 0, \tag{11}$$

for $i = x, y, z$, from which $\widehat{\mathbf{w}}^{n+1}$ and $\widehat{\mathbf{v}}^{n+1}$ can be computed according to step 3 and 4 in Problem 2.

To assemble and solve the resulting system, we use the FEM-toolbox AMDiS[38,39] with domain decomposition on 16 processors. As a linear solver, we have used a BiCGStab(l) method with $l = 2$ and a Jacobi preconditioner with ILU(0) local solver on each partition.

C. Comparison and validation

Both approaches lead to the same results. However, the computational cost for Problem 2 is drastically reduced. To quantify this reduction, we compare the assembly time for the second order operators in Problem 1 and Problem 2. We consider a sphere as a computational domain $\mathcal{S} = \mathbb{S}^2$ and vary the triangulation $\mathcal{T}$. Figure 1 shows the assembly time as a function of degrees of freedom (DOFs). The time is the mean value of multiply runs of the assembly routine. The results indicate a reduction by a factor of approximately 50.

We now compare the solution of Problem 2 with an example considered in Ref. 26 using DEC. It considers a nontrivial solution with $\text{div}_{\mathcal{S}} \mathbf{v} = 0$ and $\text{rot}_{\mathcal{S}} \mathbf{v} = 0$. Such harmonic vector fields can exist on surfaces with $g(\mathcal{S}) \neq 0$. We consider a torus which has genus $g(\mathcal{S}) = 1$. A torus can be described by the level-set function $T(\mathbf{x}) = (x^2 + y^2 + z^2 + R^2 - r^2)^2 - 4R^2(x^2 + z^2)$ with $\mathbf{x} = (x, y, z) \in \mathbb{R}^3$, major radius R and minor radius r. We here use $R = 2$ and $r = 0.5$. Let ϕ and θ denote the standard parametrization angles on the torus. Then, the two basis vectors can be written as $\partial_\phi \mathbf{x}$ as well as $\partial_\theta \mathbf{x}$ and

read in Cartesian coordinates $\partial_\phi \mathbf{x} = (-z, 0, x)$ as well as $\partial_\theta \mathbf{x} = (-\frac{xy}{\sqrt{x^2+z^2}}, \sqrt{x^2 + z^2} - 2, -\frac{yz}{\sqrt{x^2+z^2}})$. There are two (linear independent) harmonic vector fields on the torus,

$$\mathbf{v}_\phi^{harm} = \frac{1}{4(x^2 + z^2)} \partial_\phi \mathbf{x} \quad \text{and} \quad \mathbf{v}_\theta^{harm} = \frac{1}{2\sqrt{x^2 + z^2}} \partial_\theta \mathbf{x}.$$

The example considers the mean of the two harmonic vector fields as initial condition $\mathbf{v}_0(\mathbf{x}) = \frac{1}{2}(\mathbf{v}_\phi^{harm} + \mathbf{v}_\theta^{harm})$ and shows the evolution towards a Killing vector field which is proportional to the basis vector $\partial_\phi \mathbf{x}$. The surface Reynolds number is $\text{Re} = 10$. Figure 2 shows the results obtained with the fully discrete scheme of Problem 2 with time step width $\tau_n = 0.1$ and penalization parameter $\alpha = 3000$ on the same mesh as
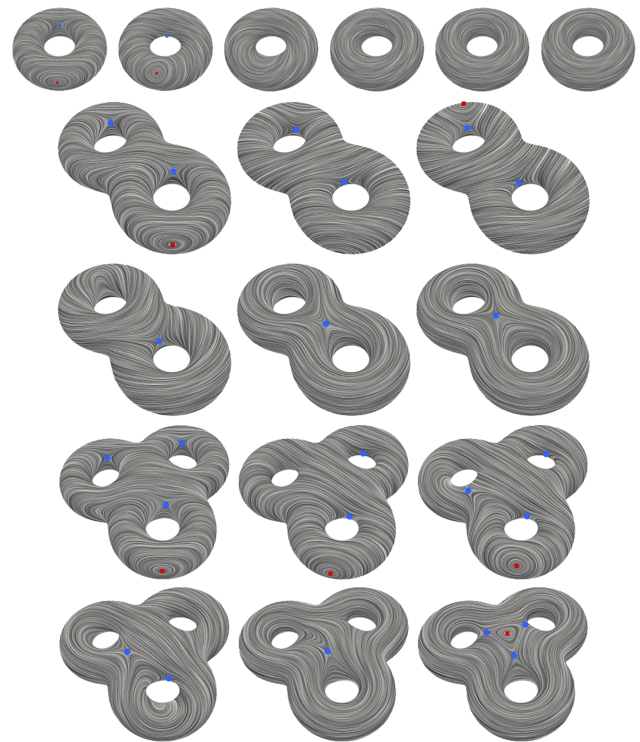

FIG. 4. Numerical solution of $\widehat{\mathbf{v}} = -\boldsymbol{\nu} \times \widehat{\mathbf{w}}$ for the 1-torus (top row) at $t = 0, 5, 10, 15, 25,$ and 100 (left to right), the 2-torus (2nd and 3rd row) at $t = 0, 10, 20, 30, 50,$ and 100 (left to right) as well as the 3-torus (4th and 5th row) at $t = 0, 10, 20, 30, 50,$ and 100 (left to right) visualized as noise concentration field aligned to the velocity field $\widehat{\mathbf{v}}$. The red squares and blue circles indicate +1 defects (vortices) and –1 defects (saddles), respectively. The full evolu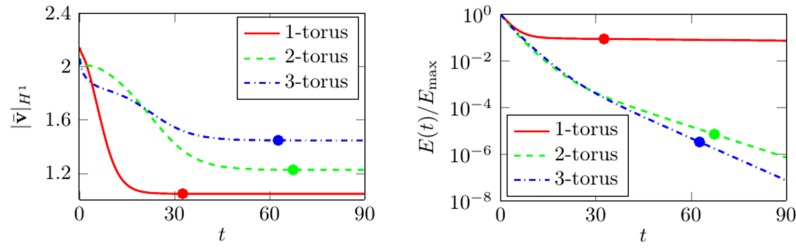tion for the three examples is provided. Multimedia views: https://doi.org/10.1063/1.5005142.1; https://doi.org/10.1063/1.5005142.2; https://doi.org/10.1063/1.5005142.3

FIG. 5. H^1 semi-norm of the rescaled velocity field $\bar{\mathbf{v}} = \widehat{\mathbf{v}}/\|\widehat{\mathbf{v}}\|_{L^2}$ against time t (left) and normalized kinetic energy $E/E_{\max}$ against time t (right), where $E_{\max}$ is the maximum value of the kinetic energy E over time. The colored dots indicate the time points at which the defects reach their final position and only viscous dissipation takes place or a Killing vector field is formed. We identify these points if the decay rate of the H^1 semi-norm of the rescaled velocity field $\bar{\mathbf{v}}$ reaches 0.001% of its maximum value over time.

considered in Ref. 26. For the Gaussian curvature κ, we use the analytic formula.

In Fig. 3 (left), we compare $\widehat{\mathbf{v}}$ with $\widehat{\mathbf{v}}^{\text{DEC}}$ for various α, thereby $\widehat{\mathbf{v}}^{\text{DEC}}$ is the solution $\mathbf{v}$ of Eqs. (1) and (2) with zero normal component from Ref. 26. Again first order convergence in α can be obtained. In Fig. 3 (right), we consider the rescaled velocity field $\bar{\mathbf{v}} = \widehat{\mathbf{v}}/\|\widehat{\mathbf{v}}\|_{L^2}$ in order to show that the penalization of the normal component $\bar{\mathbf{v}} \cdot \nu$ is numerically satisfied. For fixed α, the same convergence properties in space and time are found as in flat geometries with periodic boundary conditions.[9]

IV. RESULTS

The Poincaré-Hopf theorem relates the topology of the surface to analytic properties of a vector field on it. For vector fields $\mathbf{v} \in T\mathcal{S}$ with only finitely many zeros (defects), it holds that $\sum_{\mathbf{x} \in \mathbf{v}^{-1}(\mathbf{0})} \text{Ind}_{\mathbf{x}}\mathbf{v} = 2 - 2g(\mathcal{S})$ with $\text{Ind}_{\mathbf{x}}\mathbf{v}$ being the index or winding number of $\mathbf{x}$ for $\mathbf{v}$ and $g(\mathcal{S})$ being the genus of the surface $\mathcal{S}$. To highlight this relation, we consider n-tori for $n = 1, 2, 3$ with genus 1, 2, and 3, respectively. Obviously, the simulation results have to fulfill the Poincaré-Hopf theorem in each time step, but they will also provide a realization of the theorem which depends on geometric properties and initial condition. Similar relations have already been considered for surfaces with $g(\mathcal{S}) = 0$ in Refs. 26 and 31.

A general form of a level-set function for a n-torus can be written as $L(\mathbf{x}) = \prod_{i=1}^{n} T(\mathbf{x} - \mathbf{m}_i) - (n - 1)\delta$ with a constant $\delta > 0$ and the midpoints of the tori $\mathbf{m}_i \in \mathbb{R}^3$ for $i = 1, \ldots, n$. In the following examples, we consider the fully discrete scheme for Problem 2 and use Re $= 10$, $\tau = 0.1$, $\alpha = 3000$, $R = 1$, and $r = 0.5$. For the Gaussian curvature κ, we use the analytic formula. The initial condition is considered to be $\mathbf{v}_0 = \text{rot}_{\mathcal{S}}\psi_0 = \nu \times \text{grad}_{\mathcal{S}}\psi_0$ with $\psi_0 = \frac{1}{2}(x + y + z)$ which ensures the incompressibility constraint.

Figure 4 (Multimedia view) (top) shows the time evolution on the 1-torus with $\mathbf{m}_1 = 0$. The initial state has four defects, two vortices with $\text{Ind}_{\mathbf{x}}\mathbf{v} = +1$, indicated as red dots, and two saddles with $\text{Ind}_{\mathbf{x}}\mathbf{v} = -1$, indicated as blue dots (one vortex and one saddle are not visible). These defects annihilate during the evolution. The final state is again a Killing vector field without any defects.

For $n > 1$, the rotational symmetry is broken and Killing vector fields are no longer possible. We thus expect dissipation of the kinetic energy and convergence to $\mathbf{v} = 0$ for any

initial condition. Figure 4 (Multimedia view) (middle) shows the time evolution on a 2-torus where we have used the midpoints $\mathbf{m}_1 = (-1.2, 0, 0)$ and $\mathbf{m}_2 = -\mathbf{m}_1$ as well as $\delta = 1$. The initial state has two vortices and four saddles and thus $\sum_{\mathbf{x} \in \mathbf{v}^{-1}(\mathbf{0})} \text{Ind}_{\mathbf{x}}\mathbf{v} = -2$. Two vortex-saddle pairs annihilate each other and the final defect configuration consists of two saddles located at the center of the 2-torus (one is not visible). The velocity field decays towards $\mathbf{v} = 0$. Figure 4 (Multimedia view) (bottom) shows the time evolution on a 3-torus with midpoints $\mathbf{m}_1 = (-1.2, -0.75, 0)$, $\mathbf{m}_2 = (1.2, -0.75, 0)$, and $\mathbf{m}_3 = (0, 1.33, 0)$ as well as $\delta = 10$. Initially we have three vortices and seven saddles and thus $\sum_{\mathbf{x} \in \mathbf{v}^{-1}(\mathbf{0})} \text{Ind}_{\mathbf{x}}\mathbf{v} = -4$, which is also fulfilled for the final defect configuration with two vortices and six saddles at the center of the 3-torus (one vortex and three saddles are not visible). Again the velocity field decays towards $\mathbf{v} = 0$.

To show the differences in the evolution on the n-tori before and after the final defect configuration is reached, we consider the H^1 semi-norm of the rescaled velocity field $\bar{\mathbf{v}} = \widehat{\mathbf{v}}/\|\widehat{\mathbf{v}}\|_{L^2}$. If the defects do not move, this quantity is constant. Figure 5 shows the evolution over time together with the decay of the kinetic energy $E = \frac{1}{2}\int_{\mathcal{S}} \|\widehat{\mathbf{v}}\|^2 \, d\mathcal{S}$.

These results clearly show the strong interplay between topology, geometric properties, and defect positions.

V. CONCLUSIONS

We have proposed a discretization approach for the incompressible surface Navier-Stokes equation on general surfaces independent of the genus $g(\mathcal{S})$. The approach only requires standard ingredients which most finite element implementations can offer. It is based on a reformulation of the equation in Cartesian coordinates of the embedding $\mathbb{R}^3$, penalization of the normal component, a Chorin projection method, and discretization in space by globally continuous, piecewise linear Lagrange surface finite elements for each component. A further rotation of the velocity field leads to a drastic reduction of the complexity of the equation and the required computing time. The fully discrete scheme is described in detail and its accuracy is validated against a DEC solution on a 1-torus, which was considered in Ref. 26. The interesting interplay between the topology of the surface, its geometric properties, and defects in the flow field are shown on n-tori for $n = 1, 2, 3$.

Even if the formulation of the incompressible surface Navier-Stokes equation is relatively old,[15,22,34] numerical treatments on general surfaces are very rare. We are only

aware of the DEC approach in Ref. 26 and therefore expect the proposed approach to initiate a broader use and advances in the mentioned applications in Sec. I. We further expect it to be the basis for further developments, e.g., coupling of the surface flow with bulk flow in two-phase flow problems, as, e.g., considered in Ref. 32 using a vorticity-stream function approach or in Ref. 4 within an alternative formulation based on the bulk velocity and projection operators. Another extension considers evolving surfaces. With a prescribed normal velocity, this has already been considered in Ref. 31, again using a vorticity-stream function approach. The corresponding equations are derived in Ref. 21 using a global variational approach and in Ref. 23 as a thin-film limit. A mathematical derivation of the evolution equation for the normal component is still controversial. The derivation in Ref. 2 is based on local conservation of mass and linear momentum in tangential and normal directions, while the derivation in Ref. 20 is based on local conservation of mass and total linear momentum. The resulting equations differ. However, in the special case of a stationary surface, all these models coincide with the incompressible surface Navier-Stokes equation in Eqs. (1) and (2). In all considered examples, the Gaussian curvature was analytically given. However, this is not necessary. For appropriate algorithms to compute κ from a given surface triangulation, we refer to Ref. 27.

ACKNOWLEDGMENTS

[1]Abraham, R., Marsden, J., and Ratiu, T., *Manifolds, Tensor Analysis, and Applications*, Applied Mathematical Sciences Vol. 75 (Springer, 1988).

[2]Arroyo, M. and DeSimone, A., "Relaxation dynamics of fluid membranes," Phys. Rev. E **79**, 031915 (2009).

[3]Barrett, J., Garcke, H., and Nürnberg, R., "Numerical computations of the dynamics of fluidic membranes and vesicles," Phys. Rev. E **92**, 052704 (2015).

[4]Barrett, J. W., Garcke, H., and Nürnberg, R., "A stable numerical method for the dynamics of fluidic membranes," Numer. Math. **134**, 783–822 (2016).

[5]Bertalmio, M., Cheng, L.-T., Osher, S., and Sapiro, G., "Variational problems and partial differential equations on implicit surfaces," J. Comput. Phys. **174**, 759–780 (2001).

[6]Boozer, A. H., "Physics of magnetically confined plasmas," Rev. Mod. Phys. **76**, 1071–1141 (2005).

[7]Bothe, D. and Prüss, J., "On the two-phase Navier-Stokes equations with Boussinesq-Scriven surface fluid," J. Math. Fluid Mech. **12**, 133–150 (2010).

[8]Chorin, A., "Numerical solution of the Navier-Stokes equations," Math. Comput. **22**, 745–762 (1968).

[9]Chorin, A., "On the convergence of discrete approximations to the Navier-Stokes equations," Math. Comput. **23**, 341–353 (1969).

[10]Dörries, G. and Foltin, G., "Energy dissipation of fluid membranes," Phys. Rev. E **53**, 2547–2550 (1996).

[11]Dziuk, G. and Elliott, C. M., "Finite elements on evolving surfaces," IMA J. Numer. Anal. **27**, 262–292 (2007).

[12]Dziuk, G. and Elliott, C. M., "Surface finite elements for parabolic equations," J. Comput. Math. **25**, 385–407 (2007).

[13]Dziuk, G. and Elliott, C. M., "Eulerian finite element method for parabolic PDEs on implicit surfaces," Interfaces Free Boundaries **10**(1), 119–138 (2008).

[14]Dziuk, G. and Elliott, C. M., "Finite element methods for surface PDEs," Acta Numer. **22**, 289–396 (2013).

[15]Ebin, D. G. and Marsden, J., "Groups of diffeomorphisms and the motion of an incompressible fluid," Ann. Math. **92**, 102–163 (1970).

[16]Elcott, S., Tong, Y., Kanso, E., Schröder, P., and Desbrun, M., "Stable, circulation-preserving, simplicial fluids," ACM Trans. Graphics **26**, 4 (2007).

[17]Greer, J. B., Bertozzi, A. L., and Sapiro, G., "Fourth order partial differential equations on general geometries," J. Comput. Phys. **216**, 216–246 (2006).

[18]Hansbo, P., Larson, M. G., and Larsson, K., "Analysis of finite element methods for vector Laplacians on surfaces," e-print arXiv:1610.06747 (2016).

[19]Hu, D., Zhang, P., and Weinan, E., "Continuum theory of a moving membrane," Phys. Rev. E **75**, 041605 (2007).

[20]Jankuhn, T., Olshanskii, M. A., and Reusken, A., "Incompressible fluid problems on embedded surfaces: Modeling and variational formulations," e-print arXiv:1702.02989 (2017).

[21]Koba, H., Liu, C., and Giga, Y., "Energetic variational approaches for incompressible fluid systems on an evolving surface," Q. Appl. Math. **75**, 359–389 (2017).

[22]Mitrea, M. and Taylor, M., "Navier-Stokes equations on Lipschitz domains in Riemannian manifolds," Math. Anna. **321**, 955–987 (2001).

[23]Miura, T.-H., "On singular limit equations for incompressible fluids in moving thin domains," e-print arXiv:1703.09698 (2017).

[24]Mullen, P., Crane, K., Pavlov, D., Tong, Y., and Desbrun, M., "Energy-preserving integrators for fluid animation," ACM Trans. Graphics **28**, 38 (2009).

[25]Nestler, M., Nitschke, I., Praetorius, S., and Voigt, A., "Orientational order on surfaces: The coupling of topology, geometry, and dynamics," J. Nonlinear Sci. **28**, 147–191 (2018).

[26]Nitschke, I., Reuther, S., and Voigt, A., "Discrete exterior calculus (DEC) for the surface Navier-Stokes equation," in *Transport Processes at Fluidic Interfaces*, edited by Bothe, D. and Reusken, A. (Springer, 2017), pp. 177–197.

[27]Nitschke, I., Voigt, A., and Wensch, J., "A finite element approach to incompressible two-phase flow on manifolds," J. Fluid Mech. **708**, 418–438 (2012).

[28]Padberg-Gehle, K., Reuther, S., Praetorius, S., and Voigt, A., "Transfer operator-based extraction of coherent features on surfaces," in *Topological Methods in Data Analysis and Visualization IV*, Theory, Algorithms, and Applications, edited by Carr, H., Garth, C., and Weinkauf, T. (Springer, 2017), pp. 283–297.

[29]Rätz, A. and Voigt, A., "PDE's on surfaces: A diffuse interface approach," Commun. Math. Sci. **4**, 575–590 (2006).

[30]Reusken, A., "Analysis of trace finite element methods for surface partial differential equations," IMA J. Numer. Anal. **35**, 1568–1590 (2014).

[31]Reuther, S. and Voigt, A., "The interplay of curvature and vortices in flow on curved surfaces," Multiscale Model. Simul. **13**, 632–643 (2015).

[32]Reuther, S. and Voigt, A., "Incompressible two-phase flows with an inextensible Newtonian fluid interface," J. Comput. Phys. **322**, 850–858 (2016).

[33]Sasaki, E., Takehiro, S., and Yamada, M., "Bifurcation structure of two-dimensional viscous zonal flows on a rotating sphere," J. Fluid Mech. **774**, 224–244 (2015).

[34]Scriven, L. E., "Dynamics of a fluid interface equation of motion for Newtonian surface fluids," Chem. Eng. Sci. **12**, 98–108 (1960).

[35]Secomb, T. W. and Skalak, R., "Surface flow of viscoelastic membranes in viscous fluids," Q. J. Mech. Appl. Math. **35**, 233–247 (1982).

[36]Stöcker, C. and Voigt, A., "Geodesic evolution laws—A level-set approach," SIAM J. Imaging Sci. **1**, 379–399 (2008).

[37]Vaxman, A., Campen, M., Diamanti, O., Panozzo, D., Bommes, D., Hildebrandt, K., and Ben-Chen, M., "Directional field synthesis, design and processing," Comput. Graphics Forum **35**, 545–572 (2016).

[38]Vey, S. and Voigt, A., "AMDiS: Adaptive multidimensional simulations," Comput. Visualization Sci. **10**, 57–67 (2007).

[39]Witkowski, T., Ling, S., Praetorius, S., and Voigt, A., "Software concepts and numerical algorithms for a scalable adaptive parallel finite element method," Adv. Comput. Math. **41**, 1145–1177 (2015).